Samarium-doped thin films of the Matlockite structure: Design, luminescence, and hole-burning experiments

Monnier, Alain; Schnieper, Marc; Jaaniso, Raivo; Bill, Hans

Samarium-doped thin films of the Matlockite structure: Design, luminescence, and hole-burning experiments

A. Monnier[a] and M. Schnieper
Department of Physical Chemistry, University of Geneva, 30 Quai E. Ansermet, 1211 Genève, Switzerland

R. Jaaniso
Institute of Physics, Riia maantee 142, EE-2400 Tartu, Estonia

H. Bill[b]
Department of Physical Chemistry, University of Geneva, 30 Quai E. Ansermet, 1211 Genève, Switzerland

(Received 10 October 1996; accepted for publication 16 April 1997)

The growth of thin films made from Samarium-doped alkaline earth fluoro halides (AEFH) of composition $Sr_xCa_{1-x}FCl:Sm^{2+}$ $(0 \leqslant x \leqslant 1)$ is presented and the possibilities are studied to increase significantly the inhomogeneous width of the Sm^{2+} optical zero phonon transitions. The best films were obtained when grown with a molecular beam deposition (MBD) method involving two separate molecular beams: one for the alkaline earth fluoride, the other one for the alkaline earth halide (Cl or Br). The results demonstrate that the double beam MBD technique employed is able to produce pure and mixed Matlockite films with targeted composition. The results of mainly optical studies of the samarium $f-f$ transitions and of other complementary techniques are used to assess the composition and homogeneity of the films. With the aid of a model the composition dependence of the positions of specific optical $f-f$ emission lines is established. Their inhomogeneous linewidth is compared with that of corresponding emission lines obtained from bulk samples of the same chemical composition. The linewidths of the films are only slightly larger ($\sim 1.5-2$ times). Thus, the film morphology cannot be exploited to increase substantially the inhomogeneous broadening of the luminescence lines. A novel approach to increase this broadening was devised, theoretically modeled and successfully tested by using multilayered sandwich-type thin films in conjunction with interdiffusion. Films with cation disorder of composition $Sr_xCa_{1-x}FCl$ ($x=0.5$ /0/ 0.5/ 0/..) were grown. The $^5D_1 \rightarrow {}^7F_0$ Sm^{2+} emission linewidth is thereby increased to 70 cm^{-1} full width half maximum. A width of 100 cm^{-1} may be obtained within the composition range $x=0$, $x=1$. This represents an enhancement by a factor of 3–5 in comparison with the largest values obtained in appropriate mixed bulk AEFH of constant composition. A factor >50 is gained in comparison with pure bulk AEFH hosts. The room temperature (RT) homogeneous linewidths, on the other hand, are similar to those found in bulk mixed crystals of constant composition. The intrafilm host cation diffusion during film growth of the sandwich structures was further studied. A diffusion constant of $2 \cdot 10^{-19}$ $m^2\ s^{-1}$ for the Sr and Ca ions was deduced from this observation. These films are among the most promising materials for optical mass data storage through RT hole burning. © *1997 American Institute of Physics.* [S0021-8979(97)05314-0]

I. INTRODUCTION

Since the first reports of persistent spectral hole burning (HB) (at 4.2 K)[1,2] much research activity has developed worldwide on this subject (e.g., Refs. 3 and 4). The published demonstration of reversible room temperature HB with production of stable holes on samarium-doped mixed crystals of the PbFCl (Matlockite) family[5] represents an exciting milestone when applications of the spectral HB method are envisioned (for applications see also Refs. 3, 4, and 6), in part because up to now all HB experiments on organic systems only worked at low temperatures. In the last few years this promising result has stimulated an outgrowth of the general research effort on these systems. In particular, the mechanisms influencing the room temperature HB characteristics of the photoactive Sm^{2+} introduced into bulk Matlockite structure hosts [=alkaline earth fluorohalides (AEFH)] of composition MFX with M=Ca,Sr,Ba and X=Cl,Br are central (e.g., Ref. 7). One of the enticing properties of these hosts is to form mixed compounds of the same Matlockite structure as the pure parents (space group D_{4h}). Indeed, crystals of composition $M1_xM2_{(1-x)}FX_yY_{(1-y)}$ with M1,M2=Ca,Sr,Ba and X,Y=Cl,Br can be synthesized for any value $(0 \leqslant x, y \leqslant 1)$ of the mole fractions x,y. The partial replacement of one cation/anion species by another one of the series essentially introduces random occupation of the sites of the corresponding persisting Bravais lattices, thereby maintaining a structurally crystalline state of the compound. This intermediate disorder induces a substantial increase of the inhomogeneous optical linewidths of the Sm^{2+} [8–11] impurity incorporated into these crystals. A theoretical model[11] describes this linewidth as a function of composition. Note that a larger inhomogeneous linewidth may contain more burned holes of a given homogeneous width and thus more information can be stored. On the other hand the composi-

[a]Alain Monnier died most prematurely at the age of 34 years on August 19, 1996.
[b]Electronic mail: bill@sc2a.unige.ch

 0021-8979/97/82(2)/536/12/$10.00

tion of a chemically homogeneous and homogeneously doped sample can be predicted with the aid of the model if the numerical values of the parameters of the theory have been determined for the specific set of compounds. We apply this method in the following.

This possibility to create disorder by chemical mixing is further important in regard to the homogeneous linewidth of the holes burned. Low frequency phonons contribute importantly to its broadening at room temperature. Such phonons are, for instance, massively present in glasses where holes burned into the emission bands of Sm^{2+} impurities show sizable ($5-10\ cm^{-1}$) homogeneous broadening. On the contrary, the persistent crystal structure of the mixed AEFH presents more suitable vibrational properties in spite of the occupational disorder, yielding in comparison smaller homogeneous linewidths.[5,12] For this reason a comparatively large ratio (inhomogeneous/homogeneous) linewidth is observed in bulk mixed AEFH materials. These are at the moment among the best and most promising hosts for stable and reversible HB applications.[12] One of the ultimate goals of our contribution to this field (see also Ref. 13) is to improve the performance of AEFH related materials regarding these applications. In order to progress along this line of thinking certain questions had to be asked: can the inhomogeneous optical linewidth be enhanced by working with rare-earth (RE) doped thin films of the same materials, instead of bulk crystals, and can the homogeneous linewidth be modeled experimentally this way? Our preliminary experiments with molecular beam epitaxy (MBE) grown $CaF_2:Sm^{2+}$ films[13,14] gave strong indications that, indeed, HB properties can be substantially improved when thin films are used, rather than bulk materials. A further argument orienting our research towards thin films in view of future applications is related to their lower production costs in comparison to bulk single crystals.

As there is, to the best of our knowledge, little and indirect published material available on the growth of Matlockite type thin films it was necessary to develop appropriate growth procedures. This article gives a detailed account of the experiments, the apparatus, and the growth conditions. First, the synthesis of films of pure members of the family is described. They acted as model systems for the development of the growth methods. Then results are reported on the growth of thin films of mixed compounds and of sandwich structures. We essentially present optical results characterizing the system because our aims included the test of the basic validity of our model[11] and the acquisition of information about the suitability of these systems for HB applications. In particular we give results on the inhomogeneous linewidth of the optical bands of the Sm^{2+} impurity for the different types of films and, to a lesser extent, HB results. Our results point to the fact that the production of sandwich type mixed films can bring a truly new dimension for possible applications of the Matlockite hosts as optical storage media. We develop a model that allows the description of the inhomogeneous optical linewidths in these films with the aid of parameters of controlled diffusion experiments.

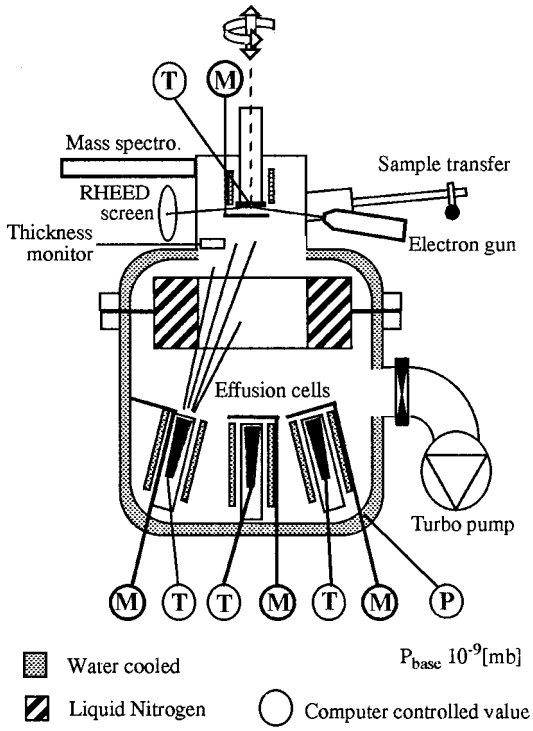

FIG. 1. Schematic view of the MBD apparatus. See Sec. II for details. Parameters controlled by computer: (M) shutter, (T) temperature, (P) pressure.

II. EXPERIMENT

A. MBD apparatus

The films were grown with an MBE apparatus built in our laboratory (Fig. 1). Since our produced films are polycrystalline, for reasons to be given later, the name molecular beam deposition (MBD) rather than MBE will be used in this article. The equipment consists of the main deposition chamber, the load-lock system, and the necessary vacuum equipment. The deposition chamber allows the use of up to five effusion cells pointing from the bottom towards to the sample holder situated at the top of the chamber. The load-lock system is attached to the main chamber for clean and easy sample manipulation. A mass spectrometer (Leybold Transpector 300) is implemented for residual gas analysis. A quartz oscillator thickness monitor (Sycon Inst. STM-100) and a modified Bayard–Alpert gauge [X-Tronix ultrahigh vacuum (UHV)] measure the beam fluxes. Finally, a reflection high energy electron diffraction (RHEED) setup (Cameca CER-1010) permits checking the surface cleanliness of crystalline substrates. The vacuum is maintained by a 400 1/s turbomolecular pump together with a 33 m^3/h primary pump. A liquid nitrogen shroud is incorporated into the growth chamber and a cryopump is connected to the latter through a high throughput UHV valve. The different parameters (pressure, temperature, water flow,..), the heaters, and the beam shutter position of each effusion cell and of the sample holder are surveyed and governed by a computer to ensure the reproducibility as well as the flexibility of the manipulation. The effusion cells (from EOSI and Mecca 2000) contain graphite crucibles coated with pyrolitic graphite. The

source materials used were CaF_2 (Merk Suprapur), SrF_2 (ultrapure, homemade from $SrCO_3$ and HF, recrystallized), $SrCl_2$ (Johnson Matthey 99%+), $CaCl_2$ (Fluka 99.5%), $SmCl_3$ (Cerac 99.9%), and SrFCl (laboratory grown from a melt of mixed SrF_2 and $SrCl_2$ powders). Crystals of the materials were first grown in our high purity Bridgman furnace and then introduced into the crucibles. The RE impurity $SmCl_3$ was directly added to the alkaline-earth chloride (AEC) during crystal growth in a nominal concentration of 1 mol %. X-ray fluorescence experiments of the Sm content yielded a typical concentration of 0.5 mol % in several as-grown films. Special precautions were taken while loading the alkaline earth chlorides into the effusion cells to avoid moisture contamination.

B. Film growth procedure

Film growth procedure includes the following steps.

(i) *Substrate cleaning and drying:* Substrates of $\sim 1\ \mathrm{cm}^2$ surface area were always used. Crystalline SrFCl, LiF, or CaF_2 plates (1.5 mm thick) were cleaved instants before their introduction into the deposition chamber. Silicon plates (1 mm thick) were cleaved from a semiconductor grade 3 in. Si wafer [(100) oriented) and cleaned according to Ref. 15]. Tantalum and molybdenum were electropolished by suitable procedures[16,17] and subsequently spin dried after a careful rinse with de-ionized water.

(ii) *Substrate transfer:* the substrate was fixed on a 2 in. molybdenum sample holder, the mount introduced into the load-lock compartment, and degassed for typically 3 h, followed by the transfer to the main deposition chamber.

(iii) *Degassing:* The temperature of the substrate was increased up to 700 °C under high vacuum. During this period, the effusion cells were progressively heated up to their standby temperature (900 °C for the alkaline earth fluorides and 600 °C for the alkaline earth chlorides). Degassing was considered to be achieved when the chamber base pressure had fallen to below 10^{-8} mbar. The liquid nitrogen shroud was then filled. Thereby the vacuum dropped typically to 10^{-9} mbar. Deposition was then initiated by bringing the effusion cells slowly to working temperature.

(iv) *Effusion cell calibration and flux adjustment:* the beam flux of each cell was calibrated while slowly scanning the cell temperature up and down. The alkaline earth chloride cell temperature was adjusted first to produce a molecular beam flux between about 3×10^{-5} moles $\mathrm{s}^{-1}\,\mathrm{m}^{-2}$ and 9×10^{-5} moles $\mathrm{s}^{-1}\,\mathrm{m}^{-2}$. Then the temperature of each alkaline earth fluoride cell was adjusted with reference to the AEC beam flux (see details below).

(v) *Growth process:* after the beam fluxes had stabilized for 1 h the computer program governing the layer growth procedure was initiated. It automatically opens and closes the appropriate cell shutters in a precise timing schedule and commands three beam flux measuring sequences: at the beginning, in the middle, and at the end of the growth process. Thereby each cell shutter is in turn opened for 5 min to measure the individual fluxes while the sample shutter is maintained constantly closed. These control sequences allowed for checking the beam flux stability during growth (typically below 2% fluctuations). The sample was removed at the end after the cells had cooled down.

(vi) *Film transfer and encapsulation:* Some of the as-grown AEFH films (especially CaFCl) are hygroscopic. To ensure their required long term stability, they were encapsulated under vacuum. The mount consists of an o-ring gasket and an optical glass window stacked over the substrate area to be protected. Assembly takes place in the deposition chamber under high vacuum, just before the sample transfer to the outside. There, the tightness of the mount is ensured by the atmospheric pressure exerted. Silicon rubber was then applied against the outside of the o-ring in order to improve the mechanical stability and the long-term tightness of the mount under the laboratory conditions.

C. Control of the fluxes

The beam flux calibration is crucial to ensure good reproducibility of the film composition. As the quartz oscillator thickness monitor is inherently unstable in the long term, we used a cross-calibration method based on the Bayard–Alpert gauge mounted on a translation arm. This gauge allowed for absolute calibration of each of the fluxes. As the stoichiometry needs to be maintained accurately, the relative beam flux(es) of the other compound(s) had to be set precisely. This can be determined rather precisely with the quartz oscillator, despite errors due to the ill-defined elastic constants of the film deposit on the quartz because these errors essentially cancel out when taking the ratio. This can be shown by starting with the general formula[18] relating the sensor frequency f and the accumulated mass per unit area m:

$$m(f,Z)=\frac{N_q D_q}{\pi z f}\arctan\left[Z\tan\left(\pi\,\frac{f_0-f}{f}\right)\right], \tag{1}$$

where $N_q=1.668\times10^3\ \mathrm{ms}^{-1}$ is the frequency constant for the given crystal, $D_q=2648\ \mathrm{kg\,m}^{-3}$ is the density of quartz, Z is a factor depending on the shear modulus of the deposited material (this value is ill-defined and subject to change for multilayered materials), and f_0 is the quart oscillator frequency prior to any deposition. The mass flux is given by

$$\dot{m}(f,Z)=\left(\frac{\partial m}{\partial t}\right)_z\frac{df}{dt}+\left(\frac{\partial m}{\partial Z}\right)_f\frac{dZ}{dt}. \tag{2}$$

The derivative dZ/dt vanishes only for a stationary flux of deposited material. However, when f is close to f_0 (say within 7.5%) and the Z factor not too great (less than 5), it can readily be shown that the accumulated mass per unit area, m, is almost independent of Z. Thus the second term of the right side in Eq. (2) can be neglected and the molecular flux ratio ϕ_i/ϕ_j, of two sources i and j may be given by

$$\frac{\Phi_i}{\Phi_j}=\frac{\dot{m}_i}{M_{wi}}\frac{M_{wj}}{\dot{m}_j}=\frac{M_{wj}}{M_{wi}}\left(\frac{\dot{f}_i}{\dot{f}_i}\right). \tag{3}$$

The conditions for f and Z are fulfilled in our experiments. Thus the relative fluxes are obtained accurately with a quartz resonator, despite the uncertainties concerning the Z factor, when the corresponding resonator frequency time derivatives, $\dot{f}_i$ and $\dot{f}_j$, are measured.

D. Luminescence and hole-burning equipment

The emission spectra of the Sm^{2+} doped films were recorded on a modified Raman spectrometer with a SPEX 1403 monochromator, a BURLE C31034-A02 photomultiplier, a Stanford Research SRS400 photon-counting system, a custom-built sample holder, and a laboratory-built PC controlled data acquisition system. Our 699 Coherent dye laser or a Spectra Physics Ar-ion laser (model 2016) provided the excitation light.

Optical narrow-band excitation and HB experiments were realized with the equipment described in Ref. 12. Colored glass filters removed the spurious light of the dye background luminescence in the excitation beam. New additions were a Hamamatsu R2949 photomultiplier and a laboratory-developed three channel photon-counting system (160 MHz bandwidth) for detection. A photodiode monitoring the laser beam was connected through an analog to digital (A/D) converter to the third channel. This allowed for normalization of the photon-counting signal by the laser output intensity. Additionally, the output power of the Coherent 699 dye laser was held constant electronically during a wavelength scan performed with the aid of a stepper motor. In the monitoring mode the nominal excitation power was about 5 mW. It was raised to about 0.5 W during burning by removal of a 20 dB attenuation filter. This latter power corresponds to a photon flux in the range of 10^5 W m^{-2} for our experimental setup.

III. PARAMETRIZATION OF INHOMOGENEOUS OPTICAL LINEWIDTHS

Configuration disorder in a solid containing impurities generally leads to enhanced width of the impurity optical bands.[19] We modified and applied this general theory by developing a detailed model of the inhomogeneous optical linewidth of Sm^{2+} in crystals with configuration disorder and applied it to the family $SrFCl_y:Br_{1-y}:Sm^{2+}$ $(0\leqslant y\leqslant 1)$.[11] Although the general principles given are straightforwardly extendible to other families, for instance to $Sr_xCa_{1-x}FCl:Sm^{2+}$ which is of particular interest in the following, for computational reasons we preferred to use a simplified approach of the general solution. Based on Eq. (17), Ref. 11 only the first term in the cumulant expansion of the line shape was retained and a polynomial fit for the line shape and position was chosen:

$$L(\omega,x)=N_r e^{-[\omega-\omega_0(x)]^2/a\Delta\omega(x)^2},$$

with

$$\omega_0(x)=14403+143.6x-61.1x^2\ \ (\mathrm{cm}^{-1}),$$

and

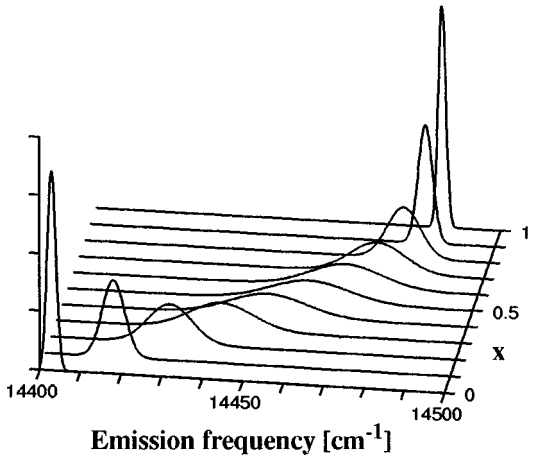

FIG. 2. Plot of the line profile $L(\omega,x)$ of Eq. (4) as a function of the molar fraction x between 0 and 1 in increments of 0.1, and of the emission frequency $\omega_0(\mathrm{cm}^{-1})$. The values of the parameters were obtained by least-square fitting Eq. (4) to the experimental $^5D_0\Rightarrow{}^7F_0$ emission band (normalized to unit integrated intensity) of Sm^{2+} in bulk crystalline $Sr_xCa_{1-x}FCl$ compounds for $0\leqslant x\leqslant 1$. The relation between x and ω_0 (of the maximum) deviates less than 2% from the experimental relation, whereas the line shape of $L(\omega,x)$ deviates from those of the experiment (e.g., Ref. 12). The line broadening is maximum near $x=0.5$.

$$\Delta\omega(x)=2.47+18.24x+272.2x^2-610.2x^3+319.5x^4\ \ (\mathrm{cm}^{-1}),$$

$$a=-\frac{1}{4}\ln\left(\frac{1}{2}\right)^{-1},\quad N_f=\frac{1}{\Delta\omega(x)\sqrt{\pi a}} \tag{4}$$

where ω_0 is the peak frequency and $\Delta\omega$ the FWHM. This approach is less precise than the full theory regarding the exact line shapes, but it is adequate for the description of the concentration dependence of the band maximum. To obtain numerical values of the parameters of the model for the $Sr_xCa_{1-x}FCl;Sm^{2+}$ compounds a set of seven crystals of compositions $x=\{0,0.3,0.5,0.7,0.9,0.95,1.0\}$ were prepared and the $^5D_0\Rightarrow{}^7F_0$ emission band of Sm^{2+} recorded.[20] These experimental results were fitted by Eq. (4) in a least square procedure. The coefficients providing the best fit are directly implemented in Eq. (4) above. With these values the maximum deviation between the experimental and the parametrized values of the band center frequency was less than 2%. The line shape function $L(\omega,x)$, resulting from this calibration is plotted in Fig. 2 as a function of the emission frequency ω (in cm^{-1}) for $0\leqslant x\leqslant 1$, in steps of 0.1. Though its detailed shape does not accurately describe the experimental line shapes for $0.3<x<0.75$ it is not detrimental for the following as we are using the *position of their (rather well-defined) maximum* to relate it to the composition x. Thereby the $^5D_0\Rightarrow{}^7F_0$ transition of the Sm^{2+} impurity of a given film of unknown composition of the $Sr_xCa_{1-x}FCl$ set is experimentally determined. Then, with the aid of Fig. 2, respectively, Eq. (4), the effective composition of the compound, can be determined. Of course the homogeneity of the film must be checked.

IV. RESULTS

A. Films of composition $SrFCl_xBr_{1-x}:Sm^2$

We started with the synthesis of these films as they have a model character for the development of a reproducible growth procedure. Another reason to start with these was that their optical luminescence and HB properties, which are of central interest to us, can be compared directly with detailed published results (e.g., Refs. 5, 9, 10, 13) obtained from bulk crystals of this same family. Initial experiments were done by growing films with the pure SrFCl compound as the molecular beam source. Several were grown this way. Insight into the homogeneity of the films during deposition was gained by growing individual ones as follows. At first the whole surface, then 2/3 and finally 1/3 was exposed to the beam, always during time intervals, Δt, of the same length obtained by precisely positioning the substrate shutter. Values of Δt were $60'$ $120'$ and $200'$, corresponding to nominal film thicknesses of 250, 480, and 950 nm in these experiments. Experiments were realized at several substrate temperatures (300, 550, and 750 °C). The encapsulated films were examined by the following methods: visual inspection under a microscope (up to 500× magnification, with polarization attachment), one film was examined with SEM and one by x-ray diffraction. Their luminescence emission was recorded. The Sm^{2+} ions dissolve uniformly into SrFCl. In the context of sample characterization we used the spatially resolved luminescence to obtain information on the chemical homogeneity of these films as the positions and the shapes of the $f-f$ emission bands are sensitive functions of the specific chemical environment of the samarium ion. This method turned out to be very useful. All of the results obtained proved that highly hygroscopic films of bad optical quality had resulted. Moreover, the sample composition varied during the deposition process. These problems were identified as being a consequence of nonstoichiometric evaporation of SrFCl, evaporating as $SrF_{2-y}Cl_y$ with $2 \geqslant y > 1$. This fact was further proved by x-ray diffraction analysis of the material remaining in the SrFCl cell crucible after a prolonged evaporation period. A new diffraction pattern, due to the formation of SrF_2, progressively appeared. The preferential evaporation of $SrCl_2$ explains both the poor material quality and the highly hygroscopic nature of these films. It also explains the change in sample composition during the cell charge lifetime.

In order to achieve reproducible film growth we undertook to synthesize the films on the substrate. Separate effusion cells, one for the alkaline earth chloride and one for the alkaline earth fluoride, were used in order to obtain a stoichiometric and stable beam composition. The justification for this successful solution is that anions and cations must necessarily evaporate stoichiometrically to maintain charge neutrality, as corroborated by residual gas analysis: no trace of Cl_2^+ or F_2^+ could be detected with the mass spectrometer during the deposition process. These films were of much higher optical quality, less hygroscopic, and of more reproducible composition than those obtained with the single cell arrangement. Films of thickness $t \cong 1$ μm were grown. Substrate temperatures below 700 °C gave the best homogeneous films with our setup. The choice of a suitable substrate was essential and several types were compared. We noticed that oxygen containing substrates such as quartz or optical glass are attacked and lead to detrimental oxygen contamination of the film. Crystal plates of CaF_2 ⟨111⟩, LiF ⟨100⟩, or SrFCl ⟨001⟩ can be used because they do not oxidize the Sm^{2+}. Useful and good quality films were obtained on tantalum, molybdenum and silicon ⟨111⟩ substrates. All three have several advantages. The handling and preparation of the substrates is very convenient. Further, there is virtually no substrate background luminescence, in contrast to the transparent ones. Then, the mirror effect increases the excitation beam path length and, consequently, the emission signal intensity, thereby enhancing its signal to noise (S/N) ratio. For these reasons most of the films were grown on molybdenum or silicon ⟨111⟩.

The characterization of the films again included visual inspection under the (polarizing) microscope, x-ray diffraction experiments, and one sample was studied by SEM. The films were found to be optically transparent, homogeneously polycrystalline with grains of microsize (the results from SEM showed the grains to be $\leqslant 200$ nm), and rather nonhygroscopic. Growth was found to be very reproducible. Even those grown on a SrFCl ⟨001⟩ substrate were polycrystalline. In this latter case homoepitactic growth had been initially expected, but it turned out that a detailed optimization of the parameters would be necessary. As this is not mandatory for our purposes, this was not done. The homogeneity of one film was further verified with the aid of the spatially resolved luminescence emission of the Sm^{2+} impurities. The surface of the film was systematically scanned with the exciting laser light and the $^5D_0 \Rightarrow {}^7F_0$ luminescence line was recorded. Within experimental precision both the line shape and the center frequency of the line were found to be independent of the position of the exciting light spot (30 μm diameter, constant power density, and excitation wavelength) scanned on a surface of 5×5 mm active area. The following aspect was used with advantage. The position and the line shape of the Sm^{2+} luminescence bands were compared with those obtained from bulk single crystals of the same composition. We found that both have the same center frequency and inhomogeneous linewidths that differed at most by a factor of 2.1. Figure 3 illustrates this point.

HB at room temperature was performed on this same sample. A hole could be burned into the $^5D_1 \Leftarrow {}^7F_0$ band of the film. Figure 4 presents the excitation profile of the $^5D_1 \Leftarrow {}^7F_0$ line, monitored on the $^5D_0 \Rightarrow {}^7F_0$ emission, before and after the HB experiment. It further shows the difference spectrum. After 10 s exposure time a remarkably deep (20%) hole of a width at half height $\Delta\overline{\nu} \cong 3.2$ cm^{-1} had formed. This result compares very favorably with those obtained on bulk single crystals of this compound, where typically 5% deep holes of the same width resulted after an exposure time of 1 min (see e.g., Refs. 5, 12, and 13). To summarize, the line position is at the same frequency and the inhomogeneous linewidth is somewhat larger in the films than in a bulk solid of the same composition, whereas the homogeneous linewidth is of comparable magnitude.[12] The detailed nature of the underlying electron transfer mechanisms in the

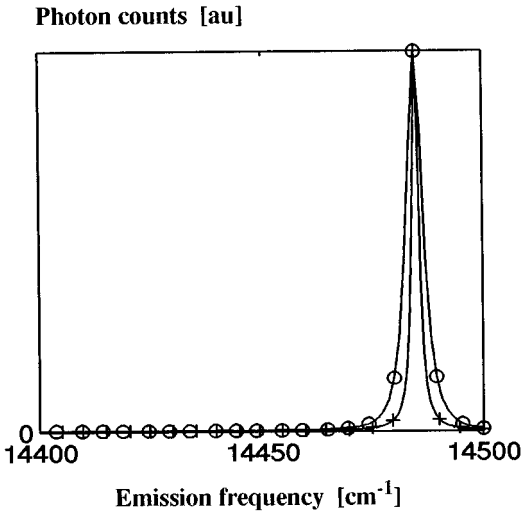

FIG. 3. Experimental $^5D_0 \Rightarrow {}^7F_0$ emission line of a pure SrFCl;Sm^{2+} film (○) at room temperature together with the corresponding line obtained from a bulk single crystal of the same composition (+). The line positions are identical but the linewidth of the film is broader by a factor of approximately 2. Argon ion laser excitation at 20492 cm^{-1}. (The marks identify each of the two line traces.)

films seems to be quite complex and work on this subject is in progress.

B. $Sr_xCa_{1-x}FCl:Sm^{2+}$

The results of the above section show that the optical investigation must be extended to mixed films. We chose to synthesize films of this family of compounds. Mixed films of composition $x=0.4$, 0.5, and 0.65 were grown with the same double cell arrangement described above by simply replacing the SrF_2 source by a CaF_2 source. The substrate temperature was 790 °C. The important question on the crystallinity of the films was also addressed for this family. Several films were examined by the same methods as described above for the SrFCl films. The result is that the films are also microcrystalline. They are transparent and show a granulation smaller than the wavelengths of the visible light. Further, they were found to be homogeneous.

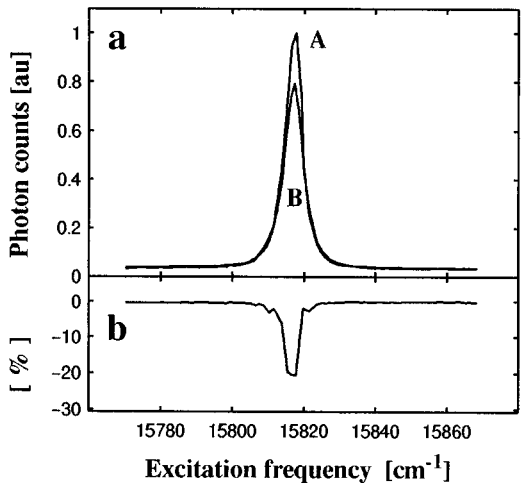

FIG. 4. Experimental $^5D_1 \Leftarrow {}^7F_0$ excitation profile (monitored with the aid of the $^5D_0 \Rightarrow {}^7F_0$ emission) of Sm^{2+} in a thin film of composition SrFCl, RT. Resolution of the monochromator set to 1 cm^{-1}. (a) Trace A: intensity $I_A(\omega)$ before burning a hole, trace B: $I_B(\omega)$ after hole burning. (b) The burned hole. The scale is $[I_B(\omega)-I_A(\omega)]/I_A(\omega)$ expressed in %.

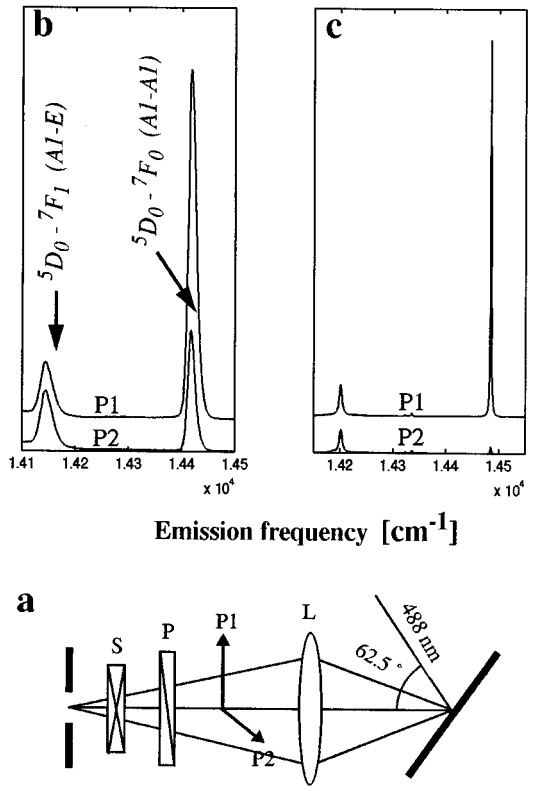

FIG. 5. Fluorescence polarization of the transitions $^5D_0 \Rightarrow {}^7F_0(A_1-A_1)$ and $^5D_0 \Rightarrow {}^7F_0(A_1-E)$. (a) The experimental setup is shown in this figure. (L) lens; ($P1$) polarization vector in the reflection plane, ($P2$) same, perpendicular; (P) polarizer; (S) polarization scrambler; beam input to SPEX 1403 monochromator. Laser wavelength 488 nm. Optical axis of the detection path horizontal in the drawing. Laser beam orthogonal to the film surface. (b) Fluorescence polarization of the film $Sr_xCa_{1-x}FCl:Sm^{2+}$ ($x=0.4$ nominally), and (c) (for comparison) of a SrFCl:Sm^{2+} film (labeling not repeated).

To obtain information regarding the orientation of the crystallites we performed fluorescence polarization measurements on a film $Sr_{0.4}.Ca_{06}FCl:Sm^{2+}$ ($t \cong 1\ \mu m$). The fluorescence emission of the $^5D_0 \Rightarrow {}^7F_0$ (A_1-A_1) and of the $^5D_0 \Rightarrow {}^7F_1$ (A_1-E) transitions was recorded at 488 nm excitation wavelength [laser 10 mW, unfocused and directed along the surface normal, see Fig. 5(a) for the geometry of the experiment]. If the crystallites are not fully randomly oriented the polarization properties of these transitions should be different as the $A_1 \Leftrightarrow A_1$ transition dipole is directed along the c axis, whereas the ones of the doubly degenerate $A_1 \Leftrightarrow E$ transition are located in the plane perpendicular to c. When the sample position was oriented such that the surface normal coincided with the optical axis of the detection path, the signal was independent (within 1.5%) of the orientation of the polarizer in the detection path. The spectra shown in Fig. 5(b) were obtained with the surface normal tilted with respect to the optical axis of the detection

TABLE I. Polarization properties of mixed-cation thin films compared to the ones of a single crystal platelet placed into the same substrate holder.

Transition	Compound	P_e[a]	P[b]	Theoretical degrees of the fluorescence polarization		
				$P(c\|\|n)$[c]	$P(c\perp -n)$[d]	P(iso)[e]
A_1-A_1	CaSrFCl film	0.5	0.20...0.41	1	−0.17	0
	SrFCl crystal	0.97	0.94	1	-	-
A_1-E	CaSrFCl film	−0.02	−0.13...−0.35	−0.17	0.13	0
	SrFCl crystal	0.15	−0.19	−0.17	-	-

[a]Measured fluorescence polarization degree.
[b]True degree of fluorescence polarization.
[c]c axis is oriented along surface normal.
[d]c axis is randomly oriented in the substrate plane.
[e]Fully isotropic distribution of the crystallites.

path ($\beta=62.5°$). The spectra were measured for two mutually perpendicular polarizations P_1 and P_2. One clearly sees from Fig. 5(b) that the polarization degree is different for the $A_1 \Leftrightarrow A_1$ and the $A_1 \Leftrightarrow E$ transitions. Experiments on a bulk high quality single crystal platelet of SrFCl:Sm^{2+} were then performed in order to have a reference system. This sample was encapsulated exactly like the thin films and the c axis of the crystal pointed along the substrate normal. Figure 5(c) shows the spectra obtained from this crystal under the same polarization conditions as those used for the film. The other experimental conditions were the same as given above. The spectra shown in Figs. 5(b) and 5(c) are qualitatively similar, which points to the fact that the crystallites in the film are approximately oriented the same way as the bulk platelet in the second experiment.

For a detailed analysis it is at first necessary to eliminate the polarizing effect of the cover plate and of the crystal surface. The true degree of the fluorescence polarization is given by

$$P=\frac{P_e-P_c}{1-P_e\cdot P_c},$$

where

$$P_e=\frac{P_1-P_2}{P_1+P_2}$$

is the measured fluorescence polarization degree. P_c is the resulting degree of polarization due to the cover plate and the crystal surface. The indices of refraction were obtained by very carefully measuring the intensities of the incident, reflected, and refracted beams and by applying the Fresnel relations. The experimentally determined refraction indices $n_1=1.52$ for the plate and $n_2=1.65$ for the crystal allowed the determination of P_c. The value calculated is $P_c=0.33$ for the angle $\beta=62.5°$. The polarization of the thin film fluorescence may also be somewhat altered by scattering on the crystal surface. Therefore we performed the measurements of P_c with the aid of the unpolarized light reflected from the substrate through the film and the cover plate which yielded an experimental figure $P_c=0.22\pm0.11$. The experimental and corrected polarization degrees are presented in Table I. For comparison the theoretical values of P are further given for different orientations of the c axis. These values were obtained by assuming that the excitation through the $f-d$ vibronic states is isotropic. This assumption rests on the experimental result that the fluorescence spectra did not depend on the polarization of the 488 nm exciting laser beam at any incident angle β. Although the laser light was polarized, the excitation process can still be (quasi-) isotropic if different vibronic states involved in the absorption have different symmetry properties.

It follows from Table I that the experimental values of P for the thin film have the same sign as the values of $P(c\|n)$, i.e., the c axes are (preferentially) oriented along the substrate normal. The values of P and $P(c\|n)$ coincide within the error margins for the $A_1 \Leftrightarrow E$ transition but not for $A_1 \Leftrightarrow A_1$. The fact that the polarization degree of the $A_1 \Leftrightarrow A_1$ transition is smaller than 1 may be caused by some angular distribution centered on the substrate normal. If we assume the c axis of the crystallites to be tilted by an angle γ_0 with respect to normal, then the distribution forms a cone and the polarization degrees are governed by the formulas:

$$P(A_1-A_1)=\frac{\sin^2\beta_0(3\cos^2\gamma_0-1)}{2\sin^2\beta_0\cos^2\gamma_0+(1+\cos^2\beta_0)\sin^2\gamma_0},$$

$$P(A_1-E)=-\frac{\sin^2\beta_0(3\cos^2\gamma_0-1)}{2\sin^2\beta_0\sin^2\gamma_0+(1+\cos^2\beta_0)(1+\cos^2\gamma_0)},$$

where the angle $\beta_0=\arcsin(\sin\beta/n_2)$. The values of $P(c\|n)$ and $P(c\perp n)$ in Table I were calculated by inserting $\gamma_0=0$ and $\gamma_0=\pi/2$, respectively. By using this model distribution one can now assert that the experimental polarization degrees agree with the theoretical ones when the deviations of the c axes from substrate normal are around 25°–30°.

The question of whether the microscopic disorder of the films influences in the same way the inhomogeneous linewidths as predicted for bulk samples by our model [Ref. 12 and Eq. (4) above] was addressed by performing luminescence experiments on the $^5D_0 \Rightarrow {}^7F_0$ transition of the Sm^{2+} impurity. The emission spectrum of the film, which had nominal composition $x=0.4$, was first verified to be spatially

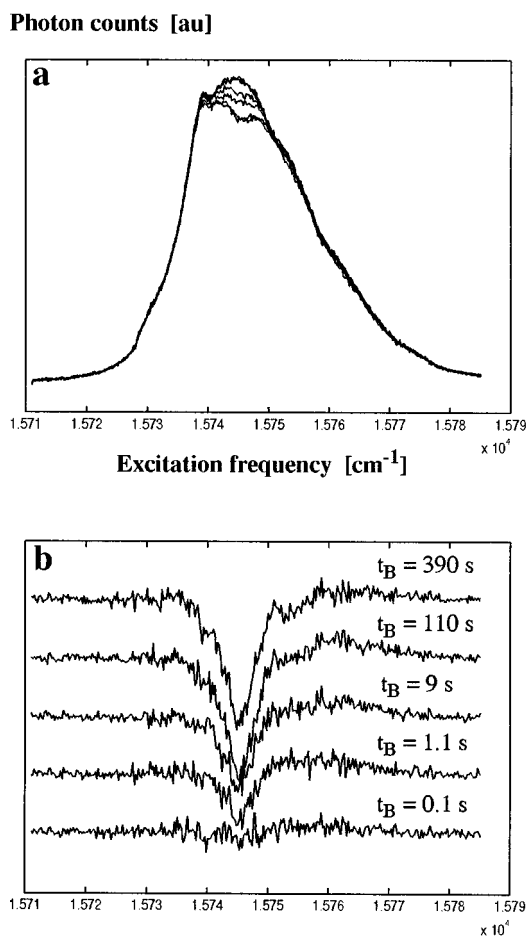

FIG. 6. Hole-burning experiment as a function of the fluence of the burning beam at constant burning intensity (expressed in time). Performed on the ${}^5D_1 \Rightarrow {}^7F_0$ transition of the same sample as used for Fig. 5. The excitation profiles were detected at wavelengths $670 \leqslant \lambda \leqslant 800$ nm (essentially with the aid of the ${}^5D_0 \Rightarrow {}^7F_0$ emission line). (a) Excitation profiles recorded after each of the totalized burning periods listed in (b). The highest maximum corresponds to $t_B = 0$ s. The lowest maximum corresponds to 390 s total duration. (b) Burned holes obtained by subtracting the unburned excitation profile from each of the other profiles shown in (a).

homogeneous (on 4×4 mm). Then the above band was recorded at a resolution better than 0.5 cm^{-1}. Its maximum was at 14447 cm^{-1}. From Eq. (4) a composition $x = 0.36$ (± 0.04) is obtained. The inhomogeneous full linewidth at half height is 22 cm^{-1}, only 4% larger than the one calculated from the model [Eq. (4)] based on bulk crystals.

A series of holes was burned on the ${}^5D_1 \Rightarrow {}^7F_0$ transition of this ($x = 0.4$) sample. Exposure times ranged from 0.1 to 390 s. The holes were detected by monitoring the luminescence emission at wavelengths greater than 670 nm under conditions described in Sec. II. Holes of a depth (Fig. 6) comparable to those found in single crystals[12] could be burned into the film at approximately 6–10 times weaker excitation intensity and at an exposure time of only 1 s, instead of 10–100 s in single crystals. Hence the quantum yield is approximately two orders of magnitude higher in the thin film than in a bulk crystal for the same transition and for identical chemical composition. A homogeneous linewidth of about 2.0 cm^{-1} is estimated from our spectra shown in Fig. 6. This is smaller by almost a factor of 2 with respect to the results given in Fig. 4.

The results given up to this point show that similar inhomogeneous linewidths are observed in both the single crystals and in thin films. To advance along the line of thought exposed in Sec. I, it was necessary to turn to the synthesis of multilayer structures as will now be described.

C. Multiple layer films

The arguments presented in Sec. V promise a total inhomogeneous broadening $> 90\ cm^{-1}$ for the system $Sr_xCa_{1-x}FCl$, over the whole composition range, i.e., a broadening larger by about a factor of 3 in comparison with the largest values attainable with a bulk single crystal (and probably also thin film) formed by a mixed AEFH of constant composition. The film growth procedure and the equipment presented above are well-suited to build up multilayer films. These can either be grown by continuous modification of the beam composition or by stepwise growth of alternating layers of defined composition. We chose to grow films of composition $Sr_xCa_{1-x}FCl$ formed by a stack of two alternating sublayers of respective compositions $x = 0$ and $x = 0.5$. These values were selected because with the effusion cells at our disposal the widest increase in linewidth[9,12] is in this way attainable. The interval $x = [0,0.5]$ gives a larger luminescence line shift between the host compounds corresponding to the two extremes than does the interval $x = [0.5,1]$. A total inhomogeneous broadening of $\sim 70\ cm^{-1}$ is expected.

Multilayers were grown as a function of the two parameters substrate temperature ($T_g = 350$, 550, and 750 °C) and sublayer thickness. The total film thickness was always kept constant (1 μm) but different numbers of stacking periods ($N = 2,10,20$) were chosen giving an individual layer thickness of $t_{sub} = 0.5$, 0.1, and 0.05 μm.

The luminescence experiments realized on the different multilayer films yielded spectra of S/N typically 50–70:1. Figure 7(a) shows the ${}^5D_0 \Rightarrow {}^7F_0$ bands of films ($N = 5$) synthesized at substrate temperatures of 350, 550, and 750 °C. The influence of the thickness of the individual sublayers is presented in Fig. 7(b) where results for films with $N = 2$, 10, and 20 are shown. The other conditions during growth were always the same. The substrate temperature T_s was 350 °C. Clearly, the diffusion processes between the layers play an important part and, depending on the precise experimental conditions, one reaches remarkably wide inhomogeneous lines. This is a clear demonstration of the effectiveness of the multilayer approach to increase the broadening. Holes were successfully burned and detected at room temperature on the absorption bands of several multilayer samples. Experimental results obtained on the sample specified by $N = 10$ and $T_s = 350$ °C of Fig. 7(b) are shown in Fig. 8. We observed (and used the fact) that holes burned into the ${}^5D_1 \Leftrightarrow {}^7F_0$ band are detected in the ${}^5D_1 \Leftrightarrow {}^7F_0$ as well as in the ${}^5D_0 \Leftrightarrow {}^7F_0$ excitation bands.

V. DISCUSSION

The initially applied method of simple thermal evaporation of the compound to grow thin films works well, of

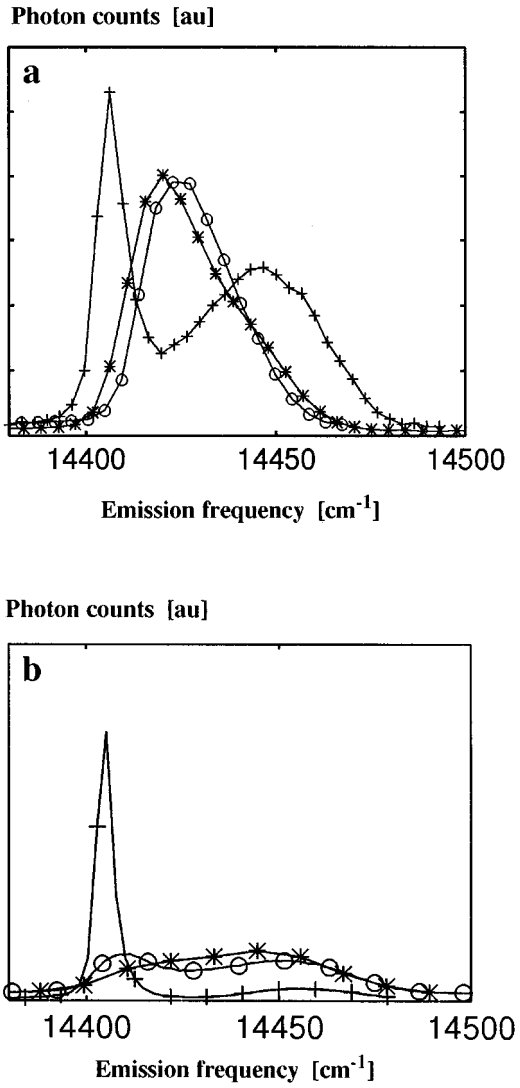

FIG. 7. $^5D_0 \Rightarrow {}^7F_0$ Sm^{2+} emission line of $Sr_xCa_{1-x}FCl:Sm^{2+}$ multilayer films. These had been grown by alternating, at equal intervals, the two compositions $x_1=0$ and $x_2=0.5$. (a) Films grown at various substrate temperatures [$T_s=350$ °C (+), 550 °C (*), and 750 °C (○)]. (b) Films of various sublayer thicknesses: [$t_{sub}=0.5$ μm (+), 0.1 μm (○), and 0.05 μm (*)], at 1 μm constant total sandwich thickness. Substrate temperature 350 °C.

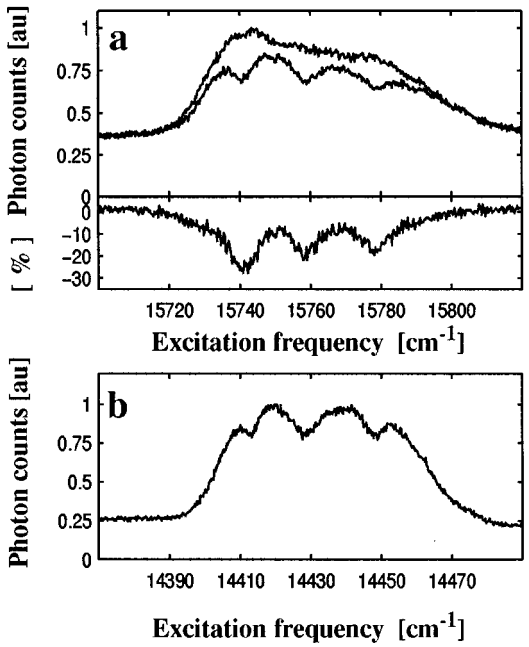

FIG. 8. Hole-burning experiment performed on two Sm^{2+} transitions of a $Sr_xCa_{1-x}FCl$: sandwich multilayer film grown at a substrate temperature $T_s=350$ °C. The film consists of alternating layers of composition $x_1=0$ and $x_2=0.5$, respectively, with a layer thickness $t_{sub}=0.1$ μm. (a) Excitation profile of the $^5D_1 \Leftarrow {}^7F_0$ transition before and after 10 s hole burning. The difference spectrum is shown below the zero line. Its intensity: [(post hole-burning intensity - prehole-burning intensity)/ prehole-burning intensity] expressed in %. The excitation profiles were detected at wavelengths $670 \leqslant \lambda \leqslant 800$ nm (essentially with the aid of the $^5D_0 \Rightarrow {}^7F_0$ emission line). (b) The holes observed on the $^5D_0 \Leftrightarrow {}^7F_0$ optical transition after they had been burned into $^5D_1 \Rightarrow {}^7F_0$ transition. The excitation profile was detected at wavelengths $720 \leqslant \lambda \leqslant 800$ nm (essentially with the aid of the $^5D_0 \Rightarrow {}^7F_1$ emission line).

course, for CaF_2 and other binary ionic compounds. But even the simplest Matlockite compound undergoes fractional distillation when heated under high vacuum. As a result one observes chemical inhomogeneity and, depending on the exact conditions, solid/solid phase separations in the grown film. This was not only observed on the SrFCl compound but we found the same effects with SrFBr and BaFCl in a preliminary experiment. A publication exists[21] where the authors report the preparation of $SrFCl_xBr_{1-x}:Sm^{2+}$ films by simple thermal evaporation. Inevitably, problems are encountered regarding the stoichiometry of the film and there is the possibility of producing mixed phases.

The pure and the mixed films of constant chemical composition yield the remarkable result that the inhomogeneous linewidth of the Sm^{2+} optical emission bands are of the same order of magnitude as those obtained from crystalline bulk hosts of the same chemical composition. To be precise, they rarely differ by more than a factor of 1.7. This is in contrast with the results on CaF_2;Sm, where an increase of the inhomogeneous linewidth by a factor 50 was observed[14] by going from the bulk crystal to a thin film. Further, the HB efficiency rose by a factor of 10. The following reasons explain this difference:

(1) the transitions are different for the two systems. For the AEFH an $f-f$ intrashell transition is observed while an intershell $d-f$ transition to the mainly $5d(T_{1u})$ excited state is involved for the AEF system. Consequently, the energy shift of the excited state levels due to a given crystal field perturbation are very different for these two systems;

(2) the CaF_2 films were grown epitactically while the AEFH films are not. The topotactic strain, induced by the epitaxy, contributes appreciably to line broadening in CaF_2;

(3) The mixed bulk AEFH are intrinsically chemically disordered and surface strains arising due to the film morphology add comparatively little to the total broadening of the AEFH.

Instead, films of these latter compounds show a behavior similar to their bulk form. The line shape is determined by the chemical disorder, in particular the local disorder of the first and second neighborhood of the Sm^{2+} impurities.[11] The individual crystallites in our films are thus sufficiently large compared to the dimensions of the local clusters so that

much of the single crystal behavior is recovered. But the similarity with the single crystal behavior is only partially accurate because there are small differences in influence on the optical emission from the films or from the bulk crystal hosts. In particular the film grain boundaries cannot be neglected in a refined treatment. Work on this aspect is in progress.

As the HB experiments presented in this article were included to demonstrate that films are suitable for RT HB work, we will not discuss this aspect in detail. This will be realized in another paper. However, the remarkable fact that the quantum efficiency in the films is definitely more favorable than in bulk crystals should be stressed. The reason for this difference is not yet fully investigated, but it is related to the existence of the grain boundaries and of electron traps in addition to the Sm^{3+} ions which are present in small quantities. The possibility of writing a hole on one transition and reading it on another one is a direct demonstration of a strong correlation between different bands. The same result was observed before for bulk host material (e.g., Ref. 5) but only through fluorescence line narrowing. The hole correlation observed in the films gives experimental evidence that the $^5D_1$ and $^5D_2$ excited levels have similar energy shifts under a given ligand field perturbation.

An interesting result of our study is the fact that thin films offer an additional and genuine way to increase inhomogeneous optical line broadening in the mixed AEFH systems when the ability of MBD to freely vary the material composition across the film is exploited. This was obtained by producing multilayer structures. The potential effectiveness of this compositional freedom was already recognized earlier due to a detailed analysis of our first luminescence emission results.[5,12,13] Figure 9 from Ref. 12 shows these results and summarizes the point. It presents the $^5D_1 \Rightarrow {}^7F_0$ luminescence emission of the Sm^{2+} impurity in various bulk AEFH compounds. As the position and shape of the $f-f$ transitions depend on the host composition and structure[11] the $^5D_1 \Rightarrow {}^7F_0$ emission lines of all the possible members of the Matlockite family plotted on a common frequency scale cover a certain spectral range as indicated in Fig. 9. Therefore, sandwich type films consisting of layers with different compositions chosen among those of Fig. 9 will show Sm^{2+} emission bands of a total inhomogeneous width given approximately by the sum of the individual widths. Our grown sandwich structure films indeed confirm this. The total observed optical emission linewidth [for instance Fig. 7(a), curve +] corresponds quite well to the prediction—as long as ionic diffusion is of minor importance. The other curves of Fig. 7(a) show that ionic diffusion between the layers introduces a gradual homogenization of the films which, for our model system, leads to a rather uniform final composition of the film with $x=0.25$. In the following section the effect of diffusion will be discussed with the aid of a model.

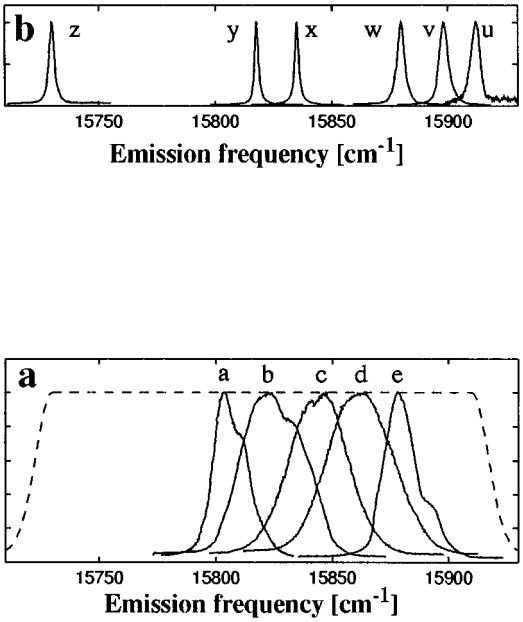

FIG. 9. $^5D_1 \Rightarrow {}^7F_0$ luminescence emission of the Sm^{2+} impurity in various bulk Matlockite structure compounds compiled on a common frequency scale. As the position and the shape of an emission line depends on the structure and composition of the individual host a whole spectral range is covered by the lines from the different hosts. The maximum spectral range encompassed by all the materials we had investigated is further indicated by a curve in Fig. 9(a). For convenience, the emission intensity maxima were arbitrarily scaled to the same value. All lines were recorded at RT. Note the sizable difference in linewidth between pure and mixed compounds. (a) Luminescence emission line of the mixed compounds (a) $Ca_{0.2}Sr_{0.8}FCl$ (b) $SrFCl_{0.5}Br_{0.5}$, (c) $Sr_{0.8}Ba_{0.2}FCl_{0.2}Br_{0.8}$, (d) $Sr_{0.5}Ba_{0.5}FCl_{0.5}Br_{0.5}$, and (e) $BaFCl_{0.5}Br_{0.5}$ (b) Luminescence emission line of the pure compounds (z) CaFCl, (y) SrFCl, (x) SrFBr, (w) BaFCl, (v) BaFBr, and (u) BaFl.

A. Modeling of the diffusion process in a sandwich structure

Modeling of the diffusion process in a sandwich structure beforehand it will be necessary to establish a quantitative relationship between the concentration profile $x(z)$ and the optical emission spectrum $\Omega(\omega)$. In the limit where reabsorption and other multiple path effects can be neglected, the spectrum is (over the full film thickness):

$$\Omega(\omega) = \int_0^{t_{\text{tot}}} C(z) S[\omega, x(z)]\, dz$$

with

$$S(\omega, x) = \sigma(x)\, \eta(x) L[\omega, x(z)], \tag{5}$$

the film is planar, z is the depth coordinate perpendicular to the plane, measured from the film vacuum interface plane, $z = t_{\text{tot}}$ corresponds to the total film thickness, and $x(z)$ is the composition profile of the film. The composition $x(z)dz$ is assumed constant within an element perpendicular to z. $C(z) = C_0$: the Sm^{2+} chromophore concentration is assumed constant throughout the film. $L(\omega, x)$ is the line shape function already defined in Eq. (4) and $\sigma(x)$ and $\eta(x)$ are the chromophore absorption cross section and quantum yield. These three functions are combined to yield the spectral function $S(\omega, x)$. The formula [Eq. (5)] is valid for an emission, excitation, or absorption spectrum, provided the elementary volume contributions to the final spectrum Ω are additive. This additivity hypothesis is restricted to systems where reabsorption and other light-scattering mechanisms

are negligible. There is an infinite ensemble of composition profiles $x(z)$ having the same spectrum $\Omega(\omega)$. Besides the spectrum, these composition profiles share a unique composition distribution function $P(x)$ defined as:

$$P(x')=\int_{z=0}^{z=t}\delta[x(z)-x']dz. \tag{6}$$

The interchangeability of integration of the integral (5) permits us to experimentally test the validity of the additivity hypothesis: any two composition profiles having the same distribution function should yield the same spectrum.

The relation [Eq. (5)] can be discretized in steps Δx and $\Delta\omega$ and written in matrix form:

$$\Omega_\omega = C_0 S^x_\omega P_x. \tag{7}$$

P_x is the vector representing the integrated thickness of the sample at a composition comprised in the interval $x-\Delta x/2$ and $x+\Delta x/2$. The sum of all the elements of P_x must be equal to the total thickness t. This formula allows for efficiently calculating the spectrum knowing the distribution function. Note that it is in principle possible to determine the composition profile corresponding to a known spectrum. However, there are some restrictions to the solutions because all the elements P_x must be positive. Thus a simple inversion of Eq. (7) is not possible, a nonlinear minimization procedure must be used instead. The next step is to modelize the diffusion effects observed on the multilayers at high substrate temperature and for thin sublayers. The film is assumed homogeneous perpendicular to z. The modulation of the strontium concentration along the z axis is represented by the function $x(z,t)$, and that of calcium by $1-x(z,t)$. Only one degree of freedom subsists as the concentrations of Ca^{2+} and Sr^{2+} are linked in order to maintain the crystal structure and charge neutrality. The homogeneity assumption does not take into account the nanocrystalline nature of the films, but it leads to a useful first approximation to describe the diffusion. The time evolution of the function $x(z,t)$ is given by the standard diffusion equation:

$$\frac{\partial^2 x(z,t)}{\partial t^2}=-D\,\frac{\partial^2 x(z,t)}{\partial z^2}. \tag{8}$$

Solving this equation by using a Fourier transform method for an initial infinite square wave composition profile, yields the following expression for this quantity as a function of time:

$$x(z,t)=\frac{1}{2}(x_1+x_2)+\frac{2S}{\pi}\left[\sum_{n=0}^{n=+\infty}\frac{(-1)^n}{2n+1}\,e^{-(2n+1)^2(t/b)}\times\cos\left(\frac{(2n+1)\pi z}{2L}\right)\right](x_1-x_2)$$

$$\text{with: } b=\frac{4S^2}{\pi^2 D}. \tag{9}$$

Thereby S is half the sublayer thickness (identical for the two species of sublayers), x_1 and x_2 are the compositions of sublayer of type 1 and type 2, respectively, D a global diffusion constant of calcium and strontium, assumed to be concentration independent. At time $t=0$, the sum in the square bracket is simply the Fourier series of the initial square wave composition profile. The exponential part damps out the contribution of order m in the Fourier series by a factor $e^{-m^2 t}$ when t increases. After a certain time, only the lowest order terms in the Fourier series remain significant. Note that Eq. (9) can be straightforwardly extended to any initial composition profile by appropriately choosing the Fourier coefficients for $t=0$. The parameter b sets the time scale of the diffusion process.

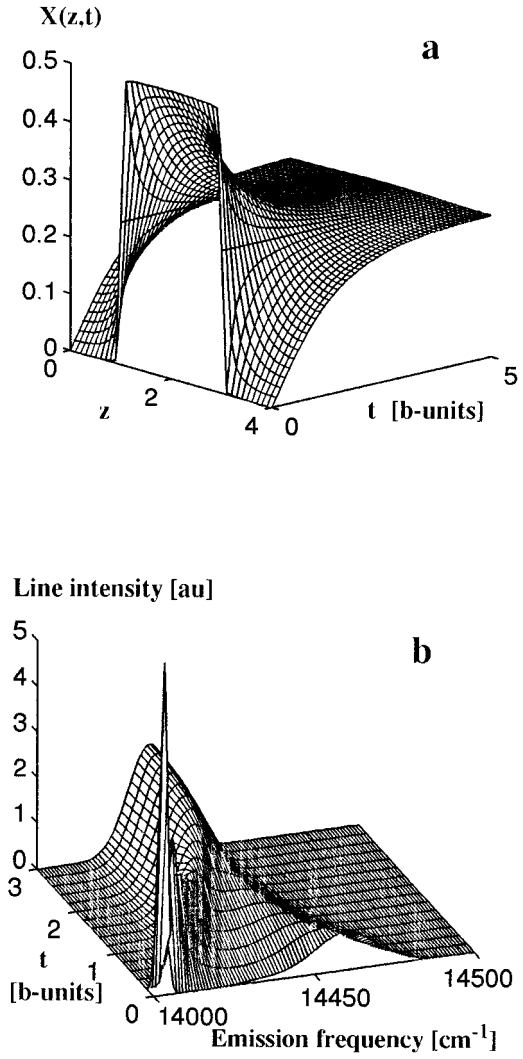

FIG. 10. (a) Time evolution of the square wave composition profile of Eq. (9). The time is given in units of $b=4\,S^2/\pi D$ and the length (z) in units of S, the sublayer half-width. For computational convenience the origin of the length scale ($z=0$) is placed at the center of the adjacent elemental layer yielding the center position at $z=2$ for the layer considered. The initial compositions are $x_1=0$ and $x_2=0.5$. (b) Calculated $^5D_0 \Rightarrow {}^7F_0$ emission line intensity (in arbitrary units) as a function of time for the composition profile displayed in (a). The spectra were calculated using Eqs. (4), (5), (6), (7), and (9). Same initial concentrations as under (a).

The time evolution profile of an initial square wave composition profile is displayed in Fig. 10(a). The corresponding optical spectra were computed by using Eqs. (4) and (9). The results are shown in Fig. 10(b) as a function of the time

expressed in units of b and of the film thickness z. Examination of this figure reveals that the collapse of the two bands is almost complete for $t \geqslant 2b$ and negligible for $t < 0.1b$, while $t = 1b$ corresponds to a partially collapsed spectrum. The important modifications of the line shape effectively take place in the vicinity of $t = 1b$. This provides a good means for an order of magnitude estimate of the parameter b, and therefore an order of magnitude value of the diffusion constant. According to Fig. 7b the transition occurs at a sublayer thickness of about 100 nm under the given growth conditions ($T_g = 350\ ^\circ\mathrm{C}$ for 3 h). When $b = 5.10^3$ s is assumed (an average value for the sublayer residence time at $T_g = 350\ ^\circ\mathrm{C}$), one obtains a value of the order of $2 \cdot 10^{-19}\ \mathrm{m^2\ s^{-1}}$ at 350 °C for D. The Einstein–Smoluchowski relation relating the jump frequency and jump length to the diffusion coefficient can be used to estimate a cation jump frequency between neighboring sites:

$$f = \frac{2D}{d^2} \tag{10}$$

With $d \cong 500$ pm the jump frequency is of the order of 1 Hz. Of course this is an approximate treatment, yet it gives some indications regarding the importance of the diffusion processes. A systematic further study will permit accurate determination of the diffusion constant as a function of temperature. In turn, this will allow the identification of the different activation processes involved in the diffusion mechanism. The diffusion processes are very important in view of the HB applications. They must be negligible at room temperature to avoid any contribution to spectral diffusion phenomena, detrimental to the long term memory properties of the material. In this respect, multilayer films constitute a very sensitive way to study the long term stability of local structures and compositions, as freshly grown films can be far from having thermodynamic equilibrium. The diffusion processes tend to move the system towards its equilibrium state. This motion is accompanied by a sharp and easily detected change of the form function of the emission spectrum of the impurities.

VI. CONCLUSION

The presented MBD approach allows the production of pure and mixed AEFH films of good quality. Further it was demonstrated that sandwich type thin films of these compounds with alternating composition can be grown, and that these show promising HB properties in view of possible applications. Besides their ability to increase the inhomogeneous broadening, the multilayered films turn out to be useful for the study of thermal diffusion phenomena. Our article shows indirectly that the development of CD disks for optical data storage at room temperature based on these materials can be promising if the advantage is used to work with multilayer films—ultimately protected by a film of pure CaF_2.

ACKNOWLEDGMENTS

D. Lovy developed the computer control of the MBE apparatus and prepared part of the figures. Dr. H. Hagemann did the luminescence experiments of the seven bulk $Sr_xCa_{1-x}FCl$ samples and Dr. F. Kubel did x-ray diffraction on a film. F. Rouge did much of the mechanical realizations. Séverine Beuchat and D. Longchamp contributed to the realization of the electronics. D. Frauchiger contributed to the substrate preparation, film growth, and did much of the maintenance of the MBE. This research was made possible by grants from the Swiss Optics Priority Program (Module I) and from the Swiss National Science Foundation. Thanks are due to both of them.

[1] A. A. Gorokhovskii, R. R. Kaarli, and L. A. Rebane, JETP Lett. **20**, 216 (1974).
[2] B. M. Kharlamov, R. I. Personov, and L. A. Bykovskaya, Opt. Commun. **12**, 191 (1974).
[3] ''Persistent Spectral Hole-burning: Science and Applications,'' edited by W. E. Moerner, in *Topics in Current Physics* (Springer, Berlin, 1988), Vol. 44.
[4] *Zero Phonon Lines and Spectral Hole-Burning in Spectroscopy and Photochemistry* edited by O. Sild and K. Haller (Springer, Berlin, 1988).
[5] R. Jaaniso and H. Bill, Europhys. Lett. **16**, 569 (1991).
[6] K. Holliday, C. Wey, M. Croci, and U. P. Wild, J. Lumin. **53**, 227 (1992).
[7] Opt. Soc. Am. Tech. Dig. **22–24** (1992)–(1994) (accounts of the Topical Meetings on Hole-burning, Ascona, Tokio).
[8] J. L. Skinner, B. B. Laird, and L. Root, J. Lumin. **45**, 6 (1990); D. L. Orth and J. L. Skinner, J. Phys. Chem. **98**, 7342 (1994).
[9] R. Jaaniso, H. Hagemann, and H. Bill, Chimia **46**, 133 (1992).
[10] R. Jaaniso, H. Hagemann, and H. Bill, Opt. Soc. Am. Tech. Dig. **22**, 79 (1992).
[11] R. Jaaniso, H. Hagemann, and H. Bill, J. Chem. Phys. **101**, 10 323 (1994).
[12] R. Jaaniso and H. Bill, J. Lumin. **64**, 173 (1995).
[13] H. Bill, R. Jaaniso, H. Hagemann, D. Lovy, A. Monnier, and M. Schnieper, Opt. Eng. (Bellingham) **34**, 2333 (1995).
[14] A. Monnier, M. Schnieper, R. Jaaniso, and H. Bill, Radiat. Eff. Defects Sol. **135**, 253 (1995).
[15] A. Ishizaka, J. Electrochem. Soc. **133**, 666 (1986).
[16] H. M. Hojka, M. Zamin, and M. K. Murthy, J. Electrochem. Soc. **126**, 795 (1979).
[17] M. Zamin, P. Mayer, and M. K. Murthy, J. Electrochem. Soc. **124**, 1558 (1977).
[18] *Sycon STM-100/MF Users Manual* (Sycon Inst. Inc. Ed., Syracuse, NY, 1993), p. 4-2.
[19] A. M. Stoneham, Rev. Mod. Phys. **41**, 82 (1969).
[20] Results communicated by Dr. H. Hagemann; See also Mater. Res. Bull. **28**, 353 (1993); *ibid.* **30**, 405 (1995).
[21] T. Asatsuma, N. Umezu, Y. Takemoto, and M. Kaneko, *Proceedings of the Topical Meeting on Hole-Burning* (AOS, Tokyo, 1995); J. Lumin. **64**, 201 (1995).